ARTICLE OPEN

Check for updates

Anisotropy oxidation behavior and mechanism of textured $Ti_3(SiAl)C_2$ ceramic

Guangqi He[1,2], Xintao Zhang[2,3], Wenting Wang[2,3], Ke Ma[2], Jun Zuo[2], Meishuan Li[2], Changsheng Liu[1] and Jingjun Xu[2]✉

Adjusting the grain growth orientation may be a feasible way to improve the oxidation resistance. In this work, textured $Ti_3(SiAl)C_2$ ceramic was successfully fabricated via the spark plasma sintering technique. The crystal orientation and microstructure were investigated by XRD combined with EBSD. The oxidation behavior of textured $Ti_3(SiAl)C_2$ was investigated at 1000–1300 °C for 10 h. The results showed that the oxidation was significantly anisotropic and the surface parallel to the compression direction exhibited better oxidation resistance below 1200 °C. The improved oxidation resistance was primarily attributed to the formation of passivated Al_2O_3 scale by rapid out-diffusion of Al elements on the orientated (*hko*) planes in textured $Ti_3(SiAl)C_2$. The formation of oxide scales was strongly dependent on the crystallographic orientation of $Ti_3(SiAl)C_2$.

npj Materials Degradation (2023)7:19 ; https://doi.org/10.1038/s41529-023-00339-4

INTRODUCTION

The ternary layered Ti_3SiC_2 is the most representative compound of $M_{n+1}AX_n$ phases, where M is a transition metal, A is a group A element, X is C or N, and $n = 1$, 2, or 3. It possesses a hexagonal crystal structure, which consists of MX lamellae and A-A atomic layer arranged in alternating stacking order along the c-axis direction. Thus, the coexistence of covalent/ionic and metallic bonds in the chemical structure allows it to combine the properties of metals and ceramics, such as low density, easy machinability, high thermal and electrical conductivity, good damage tolerance, thermal shock resistance, as well as good high-temperatures oxidation resistance, etc[1–3]. The combination of these properties makes Ti_3SiC_2 a candidate material for high-temperature structural applications.

Consequently, the high-temperature oxidation behavior of Ti_3SiC_2 has been extensively investigated in the last decade[4,5]. For example, Sun et al.[4] suggested that at 900–1100 °C, the oxide scales were composed of coarse-grained TiO_2 in the outer layer and fine-grained TiO_2 and SiO_2 in the inner layer. However, the oxidation resistance of Ti_3SiC_2 is not satisfactory above 1100 °C. Moreover, TiC always exists in Ti_3SiC_2 as impurities, which is detrimental to the high-temperature oxidation resistance. In this regard, Zhang et al.[6] introduced Al as a sintering aid into the Ti-Si-C system, which effectively inhibited the formation of TiC and also improved the oxidation resistance of Ti_3SiC_2. The improvement in oxidation resistance is attributed to the high activity and diffusivity of Al, which inhibits the inward diffusion of oxygen by forming a passivated Al_2O_3 scale during high-temperature oxidation. Normally, the added Al is present in Ti_3SiC_2 as a solid solution, i.e., $Ti_3(SiAl)C_2$.

In recent years, textured ceramic materials have attracted much attention because of their special physical and mechanical properties[7–12]. For example, Hu et al.[8] successfully fabricated textured Nb_4AlC_3 using the strong magnetic field alignment (SMFA) method combined with spark plasma sintering (SPS). The flexural strength and fracture toughness were significantly improved. Moreover, Li et al.[9] studied the oxidation resistance of textured Ti_2AlC and Ti_3AlC_2. Xu et al.[10] fabricated textured Ti_3AlC_2 by SMFA combined with the SPS technique. They found that textured Ti_3AlC_2 exhibited significantly anisotropic oxidation behavior and the surface showed better oxidation resistance along the c-axis direction. For $Ti_3(SiAl)C_2$, it possesses a hexagonal crystal structure and anisotropic properties along the a- or b-axes and c- axis. Therefore, the oxidation behavior of $Ti_3(SiAl)C_2$ can be expected to follow the anisotropy of its crystal structure. However, the process of preparing textured MAX phases by the SMFA method is complex and costly. Hence, a simple and efficient preparation method, i.e., the SPS technique, was implemented to induce grain texture of the MAX phase by loading[13,14]. The sintered MAX grains exhibit a clear preferential orientation and the obtained bulk material has mutually parallel basal planes, where a- and b-axes are randomly aligned in a plane orthogonal to c-axis and c-axis is neatly aligned.

However, most of the available works have focused on untextured $Ti_3(SiAl)C_2$, and to our knowledge, the oxidation behavior of textured $Ti_3(SiAl)C_2$ has not yet been reported. Therefore, this work aims to investigate the anisotropic microstructure and oxidation behavior of textured $Ti_3(SiAl)C_2$ fabricated by the SPS technique.

RESULTS AND DISCUSSION

Texture

Figure 1 presents XRD patterns collected from TTS and TSS samples. The diffraction peaks in all (00*l*) planes of TTS were stronger than those on TSS and standard PDF card. It suggested that (00*l*) crystallographic orientation (c-axis) was parallel to the compression direction, which indicates that the as-prepared $Ti_3(SiAl)C_2$ formed a textured structure. This texture is also verified by the diffraction peaks on TSS, which exhibited the strongest diffraction peak at $(10\bar{1}4)$, while on TTS, the strongest diffraction peak shifted to (0008), corresponding to (00*l*) planes. Based on XRD data, the Lotgering orientation factor was calculated. $f_{(00l)}$ was 0.62, which was higher than the value of Ti_3SiC_2 sintered by

[1]School of Materials Science and Engineering, Northeastern University, Shenyang 110819, China. [2]Shenyang National Laboratory for Materials Science, Institute of Metal Research, Chinese Academy of Sciences, Shenyang 110016, China. [3]School of Materials Science and Engineering, University of Science and Technology of China, Shenyang 110016, China. ✉email: jjxu@imr.ac.cn

high-temperature deformation and slip-casted in the static magnetic field, but lower than the value of Ti_3SiC_2 slip-casted in the rotating magnetic field[15,16]. In general, a larger value of $f_{(00l)}$ means a higher orientation along the compression direction. And $f_{(hk0)}$ was only 0.11, which was lower than the values of Ti_3SiC_2 slip-casted in the static and rotating magnetic fields[16]. This result suggests that the SPS technique allows alignment of the *c*-axis of the grains, but has limited control over the *a*- and *b*-axis orientations.

In addition, it can be seen that a small amount of Al_2O_3 ($2\theta = 37.77°$ and 43.35°) existed in the sample as an impurity. The presence of Al_2O_3 was unavoidable because it always existed in the prepared $Ti_3(SiAl)C_2$ powders.

Figure 2 shows SEM images of the fracture surfaces of textured $Ti_3(SiAl)C_2$. As shown in Fig. 2a, only transgranular fractures were observed and no lamellar features were present on the top surface, which is due to the weak bond between the base planes of Si or Al atoms and Ti atoms[10]. The crack propagates easily along the weak substrate plane. A typical lamellar structure can be observed on one side surface (Fig. 2b), where $Ti_3(SiAl)C_2$ grains showed a clear intercalation stacking along the c-axis. Such a tailored ceramic should have anisotropic properties along the top and side directions of the texture. This also demonstrates that SPS can prepare textured samples.

To reveal the phase distribution and grain orientation, EBSD was conducted on TSS (the acquisition surface perpendicular to the compression direction) and TTS (the acquisition surface parallel to the compression direction) surface. The phase distribution and constructed orientation maps of the grains are shown in Fig. 3. By observing the phase distribution maps (Fig. 3a, b), the red grains were identified as $Ti_3(SiAl)C_2$ phase and the blue grains as Al_2O_3 phase, which is consistent with XRD results. As shown in Fig. 3c, d, different colors indicate different grain orientations on TSS and TTS. It is noticeable that on TSS, most of the grain-exposed crystal planes were (00*l*) planes. While on TSS, there are almost no (00*l*)

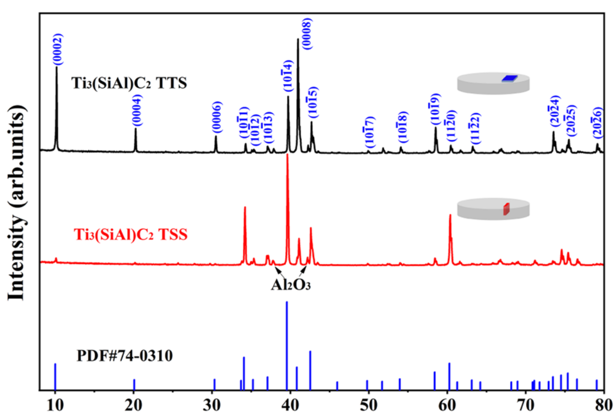

Fig. 1 XRD patterns of top and side surface of textured $Ti_3(SiAl)C_2$.

planes exposed. On the contrary, $(01\bar{1}0)$ and $(1\bar{2}10)$ planes were the main grain-exposed crystal planes.

Note that, the volume fractions of the Al_2O_3 phase in TTS and TSS were 2.86% and 4%, respectively, as determined by EBSD. The presence of Al_2O_3 also inhibited the grain growth of $Ti_3(SiAl)C_2$ during sintering. Figure 4 presents the average grain size of $Ti_3(SiAl)C_2$ particles, which was statistically about 0.98 µm for TTS and about 0.89 µm for TSS. Besides, the grain size may also be caused by the different orientations. The large grain size of TTS leads to a decrease in the number of grains observed by EBSD.

In addition, (0001), $(1\bar{2}10)$, and $(01\bar{1}0)$ pole figures derived from the stereographic projections of EBSD orientation data showed the texture orientation of TTS and TSS surfaces, as shown in Fig. 5. The highest texture intensities of TTS and TSS surfaces were 6.02 and 6.57 multiples of uniform density (MUD), respectively. These results of EBSD analysis are consistent with the orientation factors calculated from XRD data, which also demonstrates the high texture of the obtained textured $Ti_3(SiAl)C_2$ material.

Based on the above analysis, a preferential crystallographic orientation of the basal plane perpendicular to the compression direction was obtained in the as-prepared $Ti_3(SiAl)C_2$, thus providing the possibility to study its oxidation resistance.

Oxidation

To test the oxidation behavior of textured $Ti_3(SiAl)C_2$, the thermogravimetric analysis tests were conducted in air at 1000, 1100, 1200, and 1300 °C for 10 h, respectively.

Figure 6 displays the oxidation kinetics (weight change per unit area vs oxidation time) of TTS and TSS during the oxidation at different temperatures. The final mass gains at different temperatures are summarized in Table 1. The mass gain of both samples increased with increasing oxidation time. The oxidation gain curves showed a parabolic tendency below and at 1200 °C, confirming good oxidation resistance, which is consistent with the previously reported results[4]. When the temperature exceeded 1200 °C, the oxidation weight gain curves showed a linear tendency, indicating poor oxidation resistance. The TSS sample showed an overall better oxidation resistance compared to the TTS sample. After oxidation of 10 h, the weight gains of the TTS sample at 1000, 1100, 1200, and 1300 °C were 0.92, 1.60, 3.80, and 29.68 g m^{-2}, respectively. While for the TSS sample, the final weight gains were 0.54, 1.34, 3.74, and 35.43 g m^{-2} at 1000, 1100, 1200, and 1300 °C, respectively. In addition, the weight gain ratios of TTS to TSS after 10 h were 1.70, 1.19, 1.02, and 0.84 at 1000, 1100, 1200, and 1300 °C, respectively. The lower the temperature, the larger the ratio. These results revealed that texturing can improve the oxidation resistance of $Ti_3(SiAl)C_2$.

According to Fig. 6, the oxidation weight gain of textured $Ti_3(SiAl)C_2$ obeys a parabolic law at 1000–1200 °C. The corresponding square of weight gain per unit area as a function of oxidation time is shown in Fig. 7. Therefore, the correlation between the weight gain per unit area and oxidation time could

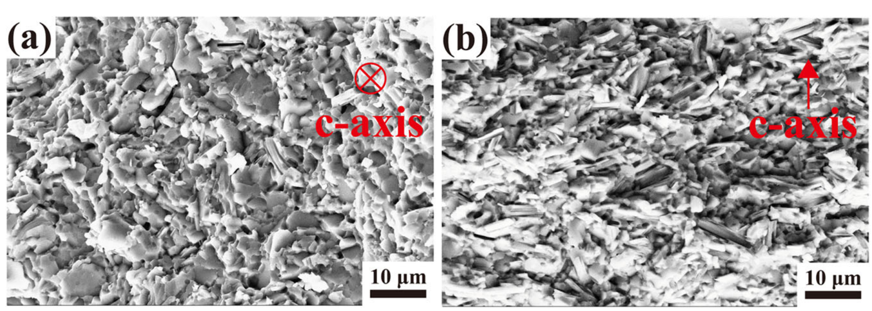

Fig. 2 **SEM images of fractured surfaces of textured $Ti_3(SiAl)C_2$.** **a** TTS sample, **b** TSS sample.

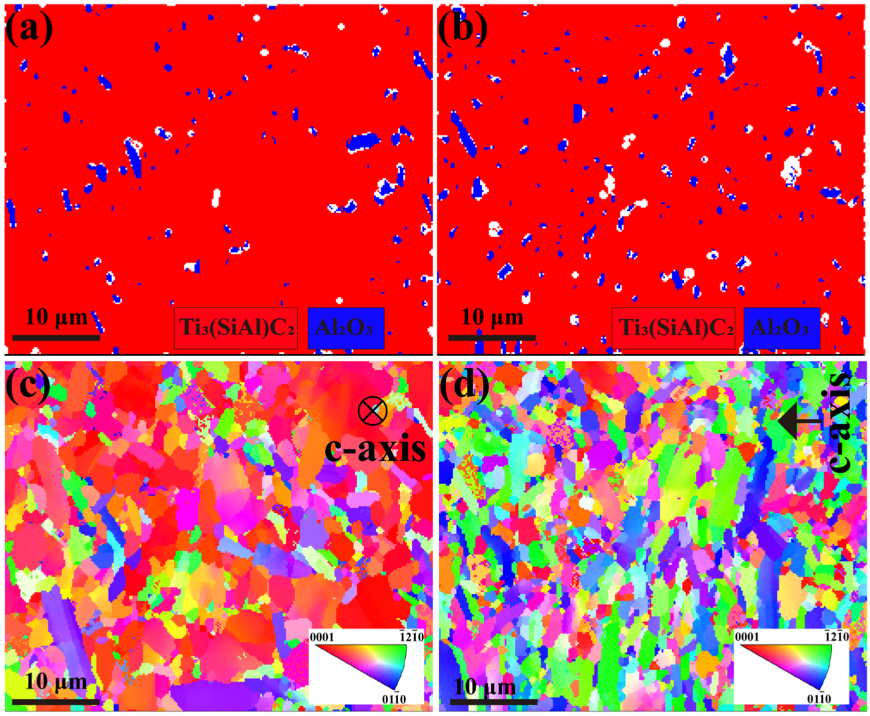

Fig. 3 EBSD characterization. Phases distribution maps of TTS (**a**) and TSS (**b**) samples. Grain orientation and Inverse pole figure (IPF) of TTS plane (**c**) and TSS plane (**d**).

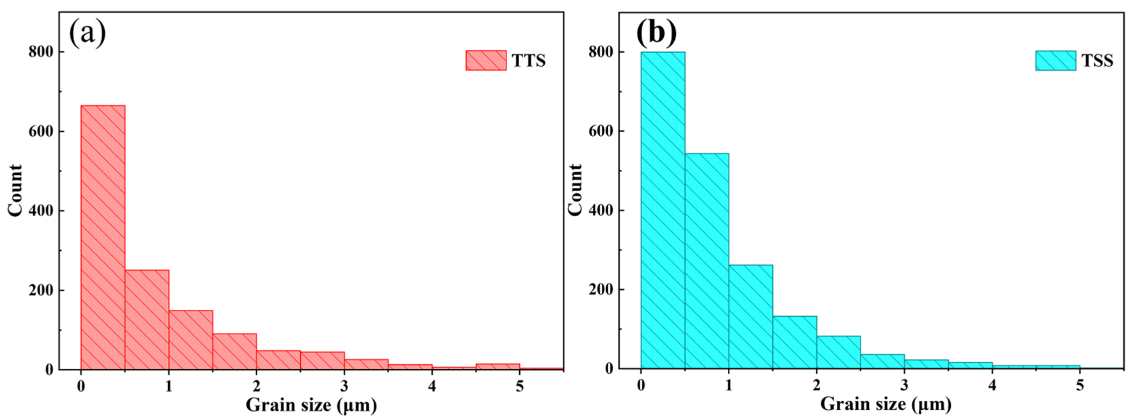

Fig. 4 The grain size of textured $Ti_3(SiAl)C_2$. **a** TTS sample, **b** TSS sample.

be described as[17]:

$$\left(\frac{\Delta W}{A}\right)^2 = k_p \cdot t \tag{1}$$

where $\triangle W/A$ is the weight gain per unit area, k_p is the parabolic rate constant, and t is the oxidation time.

When the temperature increased to 1300 °C, the oxidation weight gain of both samples deviated from the parabolic law and followed a linear law, indicating that the rate-controlling step became an oxidation reaction between $Ti_3(SiAl)C_2$ and O_2. Therefore, the correlation between the weight gain per unit area and oxidation time could be described as:

$$\frac{\Delta W}{A} = k_p \cdot t \tag{2}$$

The parabolic and linear rate constants for two samples oxidized at different temperatures are summarized in Table 2. After oxidation for 10 h, the oxidation rate constants for TTS samples were 2.4×10^{-9} kg^2 m^{-4} s^{-1}, 8.5×10^{-9} kg^2 m^{-4} s^{-1}, and 4.6×10^{-8} kg^2 m^{-4} s^{-1} at 1000 °C, 1100 °C, and 1200 °C, respectively. However, for TSS samples, the oxidation rate constants were 7.9×10^{-10} kg^2 m^{-4} s^{-1}, 5.8×10^{-9} kg^2 m^{-4} s^{-1}, and 4.4×10^{-8} kg^2 m^{-4} s^{-1} at 1000, 1100, and 1200 °C, respectively. At the same temperature, based on the total test area occupied by the faces perpendicular to the c-axis (a pair faces) and parallel to the c-axis (two pair faces), their oxidation rate constants were calculated, and also summarized in Table 2.

The relationship between the parabolic rate constant (k_p, kg^2 m^{-4} s^{-1}) and temperature (T, K) could be described by the Arrhenius' equation:

$$k_p = A \cdot \exp\left(-\frac{Q}{RT}\right) \tag{3}$$

where A is the pre-exponential factor, Q is the apparent or effective activation energy, R is the gas constant, and T is the absolute temperature. Take the logarithm on both sides of Eq. (3):

$$Ln(k_p) = Ln(A) - \frac{Q}{RT} \tag{4}$$

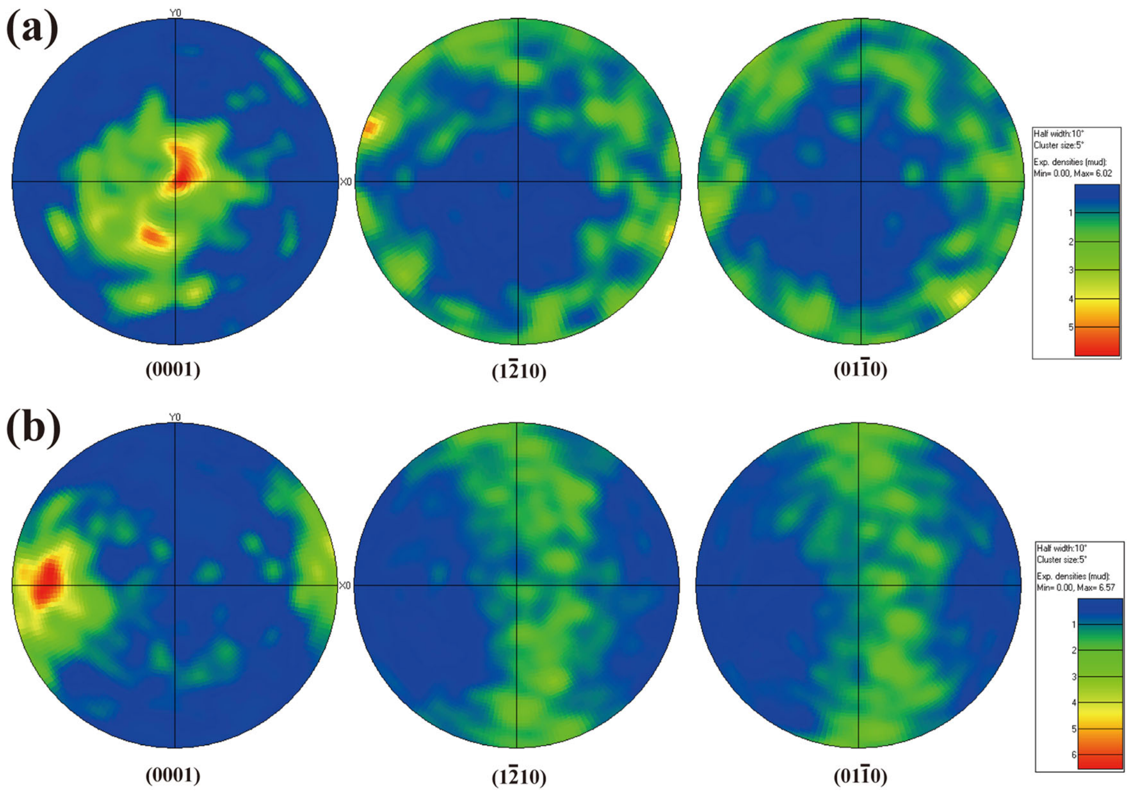

Fig. 5 The pole figure of textured $Ti_3(SiAl)C_2$. **a** TTS sample, **b** TSS sample.

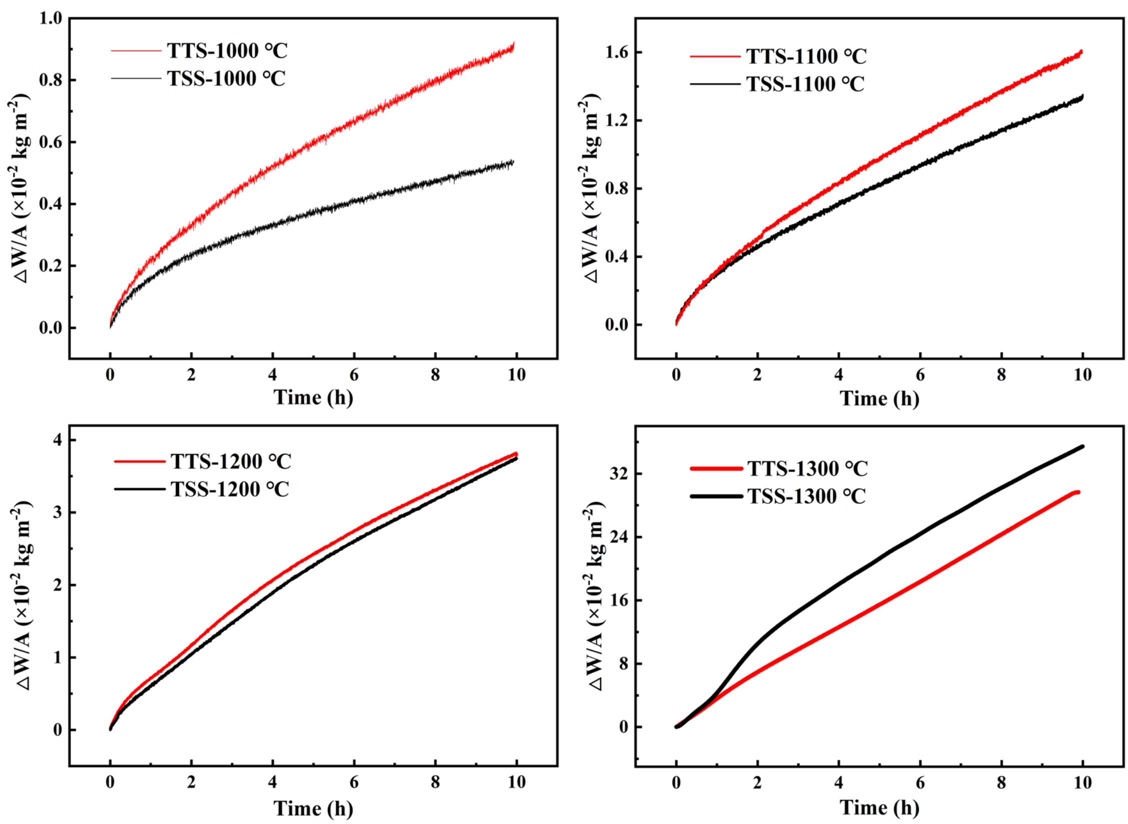

Fig. 6 The weight gain per unit area as a function of time for textured $Ti_3(SiAl)C_2$ oxidized in the temperature range from 1000 to 1300 °C.

Arrhenius plots of the logarithm of k_p for TTS* and TSS* vs the inverse of the absolute temperature are shown in Fig. 8. The data point of 1300 °C was excluded from the activation energy calculation because their oxidation pattern was deviated from the parabolic law. The values of Q were obtained from the slope of the linear fit in Fig. 8. The results show that the Q values of TTS* and TSS* were 202 ± 30 kJ mol^{-1}, and 401 ± 17 kJ mol^{-1}, respectively. The Q value of TSS* is close to 350–380 kJ mol^{-1}, which is the activation energy value for oxygen diffusion at Al_2O_3 grain boundaries[18,19]. Smialek et al.[20] studied the oxidation behavior of Al-containing MAX phases and revealed that oxygen diffusion at the grain boundaries of the Al_2O_3 scale was the primary oxidation mechanism of MAX phases. Therefore, textured $Ti_3(SiAl)C_2$ is no exception to this rule. Besides, Gao et al.[21] reported that the Q value of purity Ti_3SiC_2 was 295 ± 20 kJ mol^{-1} in the temperature range of 1150–1250 °C. A higher Q means that the oxidation rate constant of the material is more variable in the temperature range tested. However, at 1200 °C, the oxidation rate constants of the two samples were close, indicating that the lower the temperature, the greater the difference in the oxidation rate constants of the two samples. Based on the present investigation, it can be concluded that the oxidation resistance of TSS samples was superior to that of TTS samples below 1200 °C. Also, it can be inferred that the lower the temperature, the better the oxidation resistance of TSS sample.

Table 1. Summary of the weight gain per unit area (g m^{-2}) for TTS and TSS samples at different temperatures.

	1000 °C	1100 °C	1200 °C	1300 °C
TTS	0.92	1.60	3.80	29.68
TSS	0.54	1.34	3.74	35.43

Figure 9 illustrates XRD patterns of TTS and TSS oxidized samples at 1000–1300 °C. The phase compositions of the two sample surfaces at different oxidation temperatures are summarized in Table 3. It can be seen that the main phase of the TTS sample was TiO_2 at 1000 °C, while the main phase of the TSS sample was $Ti_3(SiAl)C_2$, which indicates that the thickness of the oxide layer of the TSS sample was thinner than that of TTS sample, i.e., the oxidation resistance of TSS sample was superior to that of TTS sample. At and above 1100 °C, the main phase of both samples was TiO_2, while the $Ti_3(SiAl)C_2$ phase could only be detected at 1100 °C, which indicates that the samples underwent rapid oxidation when the temperature exceeded 1100 °C. Below 1200 °C, the Al_2O_3 phase could be observed in all samples. Previous work demonstrated that the formation of a passivated Al_2O_3 layer contributes to the oxidation resistance, and it explains well the very limited weight gain of the samples below 1200 °C (see Fig. 6)[6,10]. While at 1300 °C, the diffraction peak of Al_2O_3 disappeared to be replaced by Al_2TiO_5 and the diffraction peak of

Table 2. Summary of k_p (1000–1200 °C, parabolic, kg^2 m^{-4} s^{-1}) and k_l (1300 °C, linear, kg m^{-2} s^{-1}) for $Ti_3(SiAl)C_2$.

	1000 °C Parabolic	1100 °C	1200 °C	1300 °C Linear
TTS	2.4×10^{-9}	8.5×10^{-9}	4.6×10^{-8}	8.1×10^{-6}
TSS	7.9×10^{-10}	5.8×10^{-9}	4.4×10^{-8}	8.4×10^{-6}
TTS[a]	3.5×10^{-9}	1.0×10^{-8}	4.8×10^{-8}	7.9×10^{-6}
TSS[b]	2.5×10^{-10}	4.9×10^{-9}	4.3×10^{-8}	8.5×10^{-6}

[a]A pair of faces perpendicular to the c-axis.
[b]Two pairs of faces parallel to the c-axis.

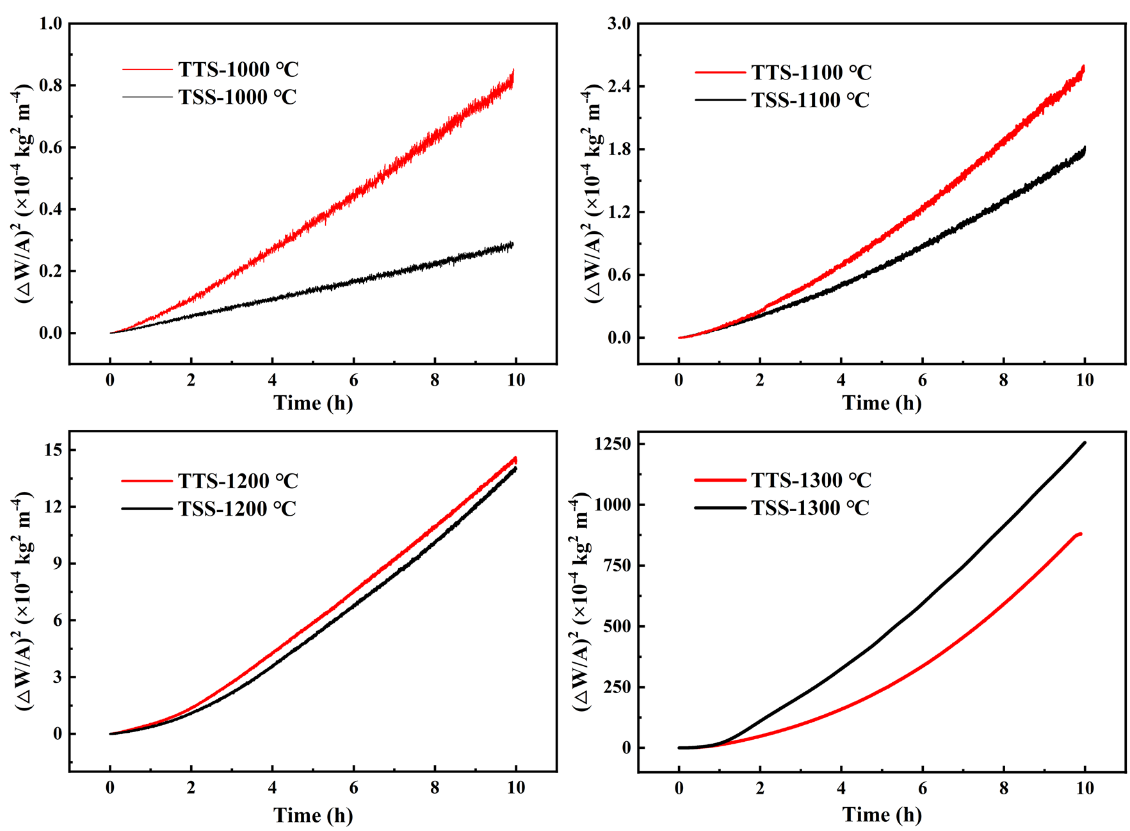

Fig. 7 Square of weight gain per unit surface area as a function of oxidation time for textured $Ti_3(SiAl)C_2$ oxidized at different temperatures.

TiO_2 (2θ = 36.1°) became significantly weaker. Al_2O_3 reacted with TiO_2 to form Al_2TiO_5, which led to the loss of the protective layer and a significant weight gain[10,22]. In addition, the TSS samples showed higher oxidation rate constants, which was also mainly because the TSS samples generated more Al_2O_3 in the initial oxidation stage, and as the oxidation time increased, Al_2O_3 reacted with TiO_2 to form Al_2TiO_5.

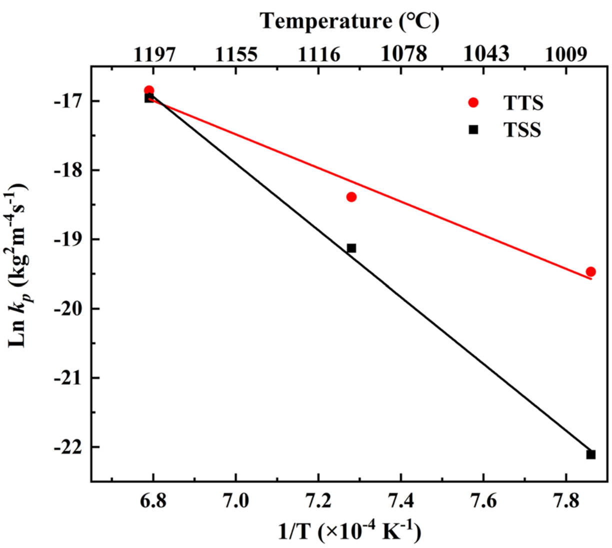

Fig. 8 Arrhenius plot of the parabolic oxidation constants for the isothermal oxidation at 1273–1573 K for textured $Ti_3(SiAl)C_2$.

Figure 10 shows the surface morphologies of TTS and TSS oxidized samples at 1000–1300 °C. It can be seen that the grain size increased significantly with the increase in temperate. Figure 10a–d shows bright TiO_2 grains dispersed on small gray Al_2O_3 grains in the oxidized samples at 1000-1100 °C. As the temperature increased to 1200 °C, TiO_2 gradually grew from small grains to large elongated crystals and no Al_2O_3 grains were observed (Fig. 10e, f). At 1300 °C, TiO_2 grew from grains to large ridge-like structures. Al_2O_3 was substituted by Al_2TiO_5, which was dispersed on TiO_2 (Fig. 10g, h). The looser or porous TiO_2 and Al_2TiO_5 scales cannot prevent further diffusion of oxygen, resulting in a rapid increase in the weight of the sample[10]. In addition, below 1200 °C, the grain size of TTS oxidized samples was larger than that of TSS samples, which corresponded well with the oxidation weight gain curve (Fig. 6). At 1300 °C, the grain size of TTS oxidized samples was smaller than that of TSS samples, which may be related to the generation of Al_2TiO_5.

To understand the oxidation mechanism of textured $Ti_3(SiAl)C_2$, the cross-sectional morphology of both samples after oxidation at

Table 3. Phase composition on the surface of TTS and TSS samples after oxidation at different temperatures.

Temperature	TTS			TSS		
	Phase compositions					
1000 °C	TiO_2	$Ti_3(SiAl)C_2$	Al_2O_3	$Ti_3(SiAl)C_2$	TiO_2	Al_2O_3
1100 °C	TiO_2	$Ti_3(SiAl)C_2$	Al_2O_3	TiO_2	$Ti_3(SiAl)C_2$	Al_2O_3
1200 °C	TiO_2	Al_2O_3		TiO_2	Al_2O_3	
1300 °C	TiO_2	Al_2TiO_5		TiO_2	Al_2TiO_5	

These phases are listed according to the peak relative intensities.

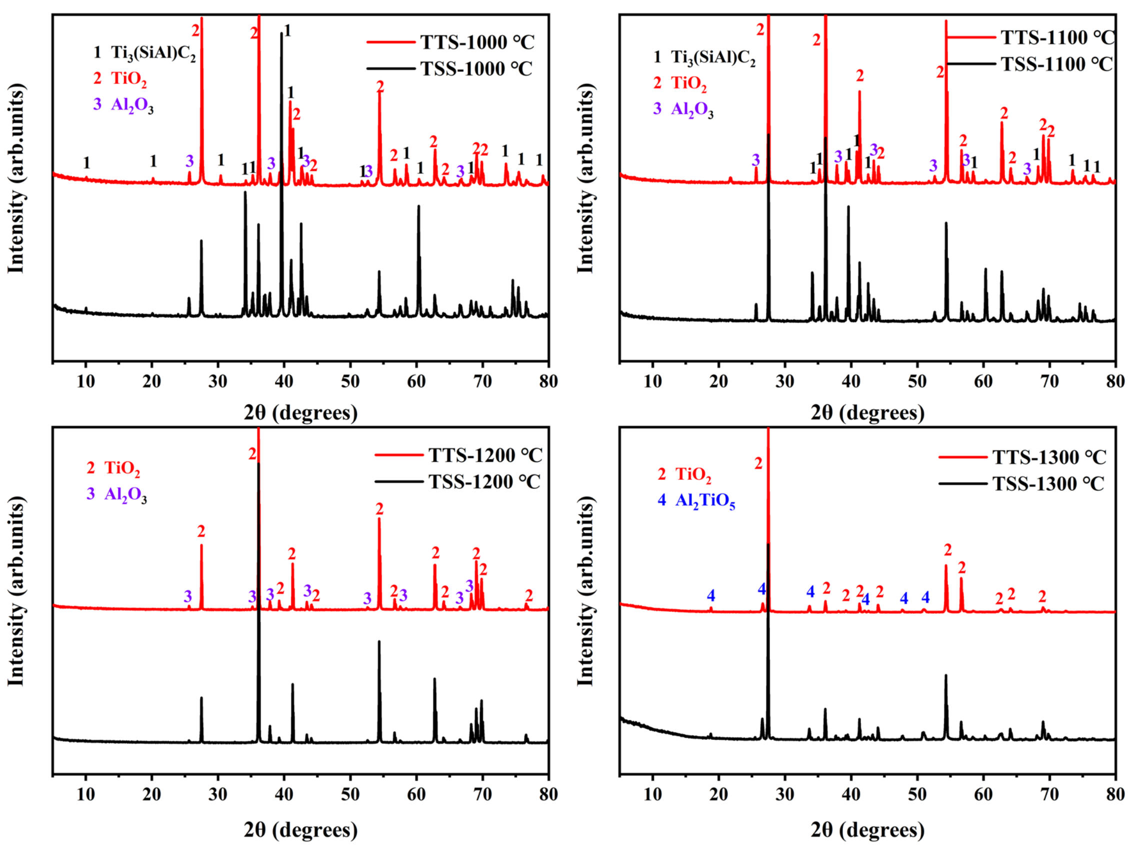

Fig. 9 XRD patterns of scales grown on textured $Ti_3(SiAl)C_2$ at different temperatures.

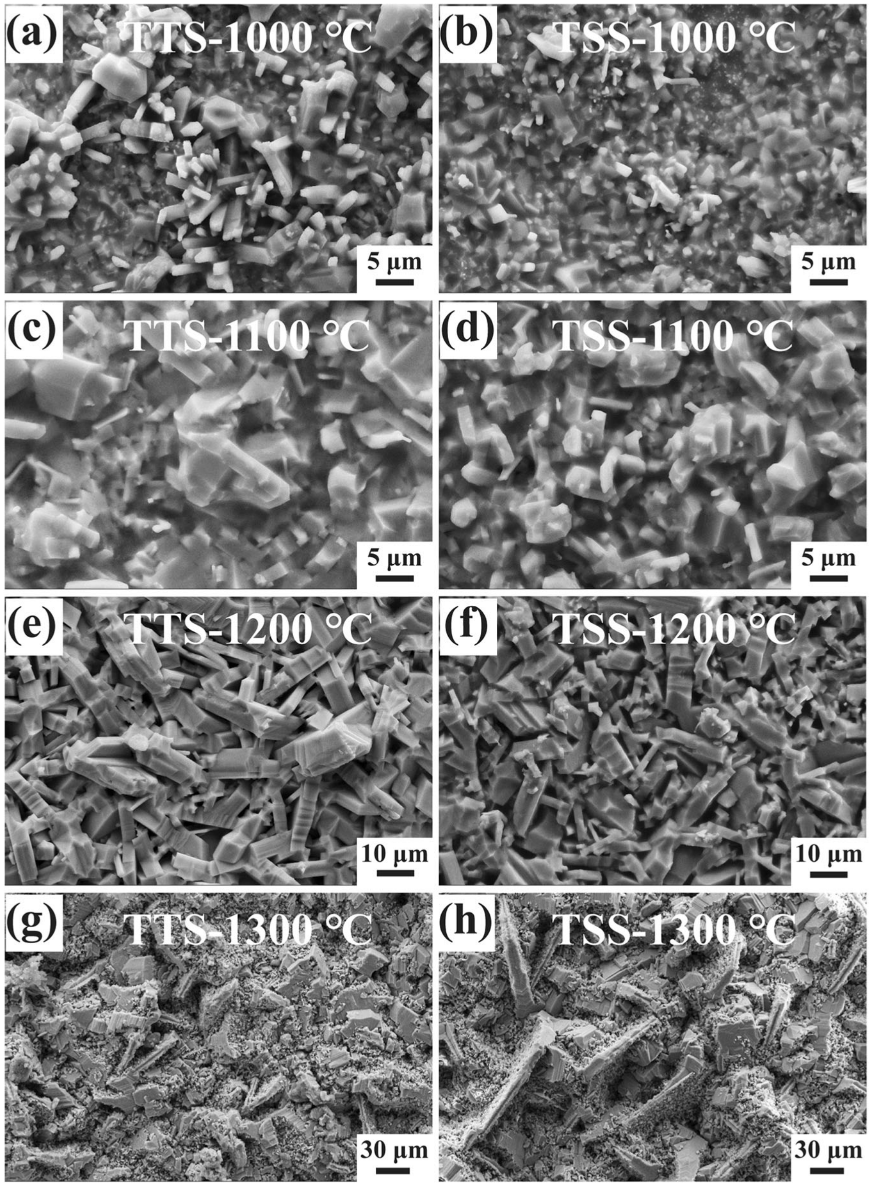

Fig. 10 SEM images of sample surfaces after the oxidation of TTS and TSS samples tested at different temperatures. **a** TTS-1000 °C, **b** TSS-1000 °C, **c** TTS-1100 °C, **d** TSS-1100 °C, **e** TTS-1200 °C, **f** TSS-1200 °C, **g** TTS-1300 °C, **h** TSS-1300 °C.

1000–1300 °C for 10 h was observed by SEM and EDS. Typical SEM images of the oxidized scales formed after oxidation at different temperatures and the corresponding EDS analysis are shown in Figs. 11 and 12, respectively. EDS images of the oxidized sample cross-sections at 1100 °C are similar to those at 1000 °C. By comparing the cross-sectional morphology of the two samples, the oxide layers of both samples showed the same multilayer structure and phase compositions at the same temperature. At 1000 °C and 1100 °C, a thin and stratified oxide layer was generated on the surface of the samples, which consisted of TiO_2 in the outer layer, Al_2O_3 in the middle layer, and a mixed layer of $TiO_2 + SiO_2$ in the inner layer. At 1200 °C, the oxide layer of the sample showed a more pronounced multilayer structure, which consisted of TiO_2 in the outer layer, an intermediate layer of Al_2O_3 interspersed inside the TiO_2 layer, and an inner layer of $TiO_2 + SiO_2$ mixed porous layer. While at 1300 °C, the oxide layer of the sample changed significantly, which consisted of an outer layer of discontinuous Al_2TiO_5, an intermediate layer of TiO_2, and an inner layer of $TiO_2 + SiO_2$ mixed layer.

On the other hand, for TTS samples, the middle layer (Al_2O_3) of the oxide layers of TTS did not connect well with the outer layer (TiO_2) and the inner layer ($TiO_2 + SiO_2$ mixed layer) with the existence of faint cracks at 1000–1200 °C, which may be due to the lack of formation of a continuous Al_2O_3 passivation layer[10]. As a result, the inner oxide layer ($TiO_2 + SiO_2$ mixed layer) was significantly thicker compared to that of TSS, as shown in Figs. 11 and 12. The oxide layer thicknesses were 12 ± 0.5 µm, 19.8 ± 3.5 µm, and 33.8 ± 2.2 µm at 1000 °C, 1100 °C, and 1200 °C, respectively. For the TSS sample, at 1000–1200 °C, it can be seen that the Al_2O_3 layer was well bonded to the outer and inner layers, and no cracks were observed. The scale thicknesses were 7.9 ± 0.9 µm, 14.4 ± 1.2 µm, and 29.2 ± 2.4 µm at 1000 °C, 1100 °C, and 1200 °C, respectively.

At 1300 °C, no Al_2O_3 phase was connecting between the outer and inner layers, resulting in significant cracks separating the inner and outer layers in both samples. This is because Al rapidly diffuses outward at high temperatures to form Al_2O_3, which reacts with TiO_2 to form Al_2TiO_5, at the same time, loses its protective

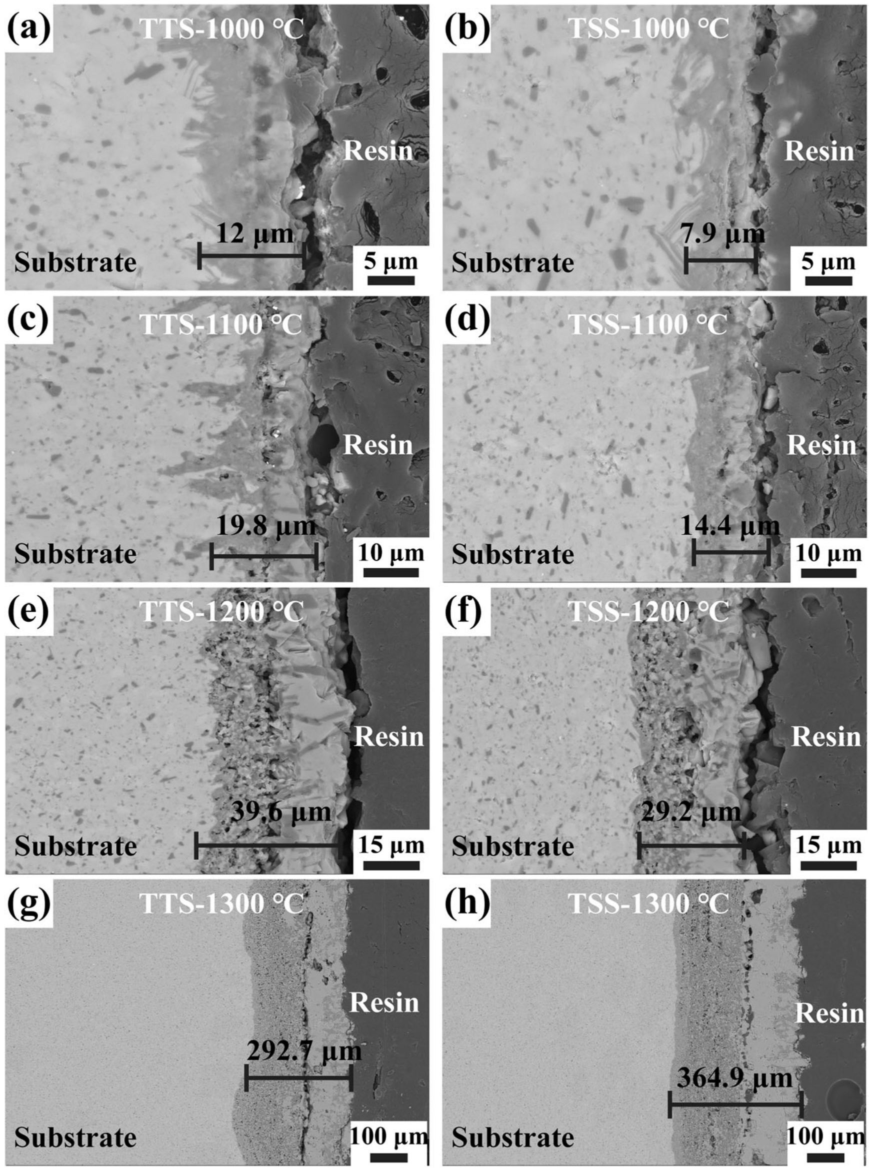

Fig. 11 SEM images of cross sections of scales grown on TTS and TSS samples tested at different temperatures. **a** TTS-1000 °C, **b** TSS-1000 °C, **c** TTS-1100 °C, **d** TSS-1100 °C, **e** TTS-1200 °C, **f** TSS-1200 °C, **g** TTS-1300 °C, **h** TSS-1300 °C.

effect on the substrate, leading to the violent oxidation of the samples. In addition, the thickness of the oxide layer of the TTS sample was lower than that of the TSS sample, which is consistent with the results in Fig. 6. In general, we can observe that higher oxidation temperatures lead to more rapid oxidation and thicker oxide layers.

Oxidation mechanism of texture $Ti_3(SiAl)C_2$

Based on the above analysis, the oxidation process of $Ti_3(SiAl)C_2$ was controlled by the inward diffusion of O and the outward diffusion of C, Ti, and Al, while Si was relatively immobile, which is in agreement with the results of the previous studies[6,23]. Therefore, the evolution of the microstructure of oxide scales and the atomistic model can be proposed to describe the formation mechanism of oxide scales on $Ti_3(SiAl)C_2$, as shown in Fig. 13.

The microstructure and growth kinetics of the different oxide scales are related to the crystallographic orientation of the crystals, as mentioned above, and the exposed grains on TTS correspond mainly to (00*l*) planes, whose planes were formed mainly by MX layers (TiC_x layers). But on TSS, most of the grains were (*hko*) planes, whose planes were formed by stacking MX layers and Si(Al)-Si(Al) atomic layers. As a result, TTS and TSS planes contain different Al contents. Moreover, Wang et al.[24] investigated the thermal stability of Ti_3AlC_2 powders at low oxygen partial pressure. The results showed that Al underwent selective oxidation on Ti_3AlC_2 and Ti_3AlC_2 powder was partially transformed into non-stoichiometric TiC_x and Al_2O_3, demonstrating the higher chemical activity of Al than other elements. For $Ti_3(SiAl)C_2$ material, the element Al can also be considered as an important element for the formation of the Al_2O_3 protective layer as a further oxidation-inhibiting layer.

For TTS samples, the (00*l*) plane was parallel to the oxide layer and the Si(Al)-Si(Al) atomic plane was perpendicular to the direction of Al diffusion, resulting in a slower diffusion of Al atoms from the (00*l*) plane to the oxide reaction layer, which had to penetrate the MX layer, thus making the growth of the Al_2O_3 layer more complicated and discontinuous. In contrast, for the TSS sample, the Si(Al)-Si(Al) atomic plane was parallel to the direction of Al diffusion, allowing rapid diffusion of Al atoms from (*hko*) plane to the oxide layer, which contributed to the formation of a continuous Al_2O_3 layer. Thus, the continuous Al_2O_3 layer can

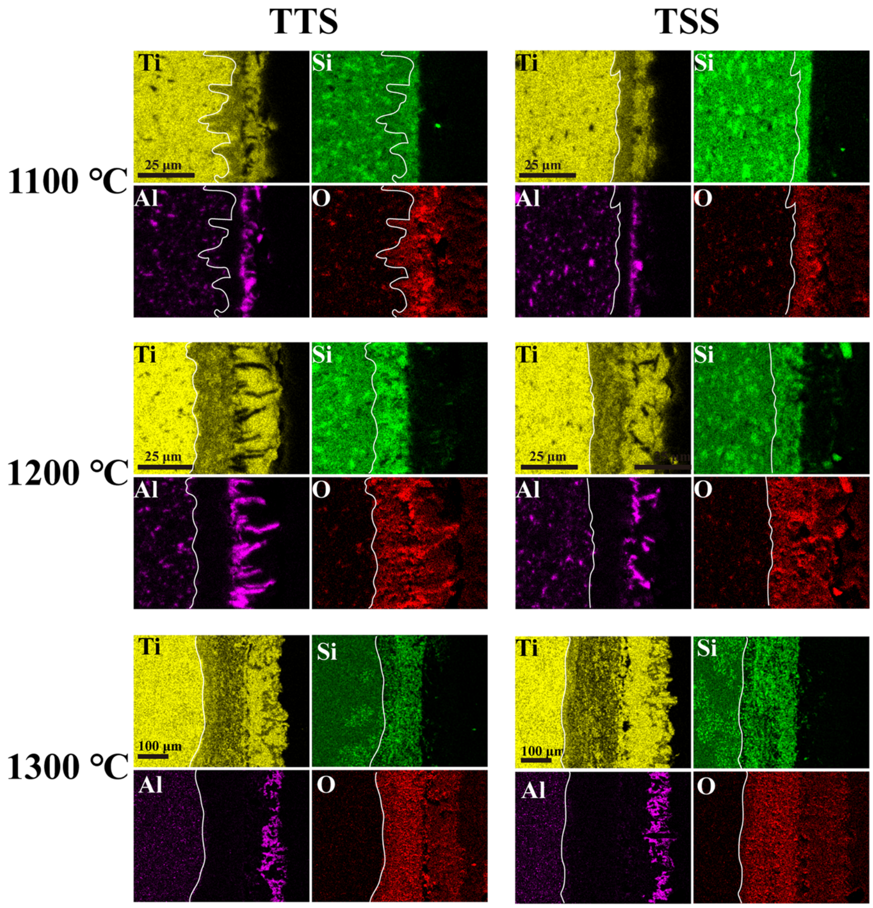

Fig. 12 EDS mappings of cross sections of scales grown on TTS and TSS samples tested at different temperatures.

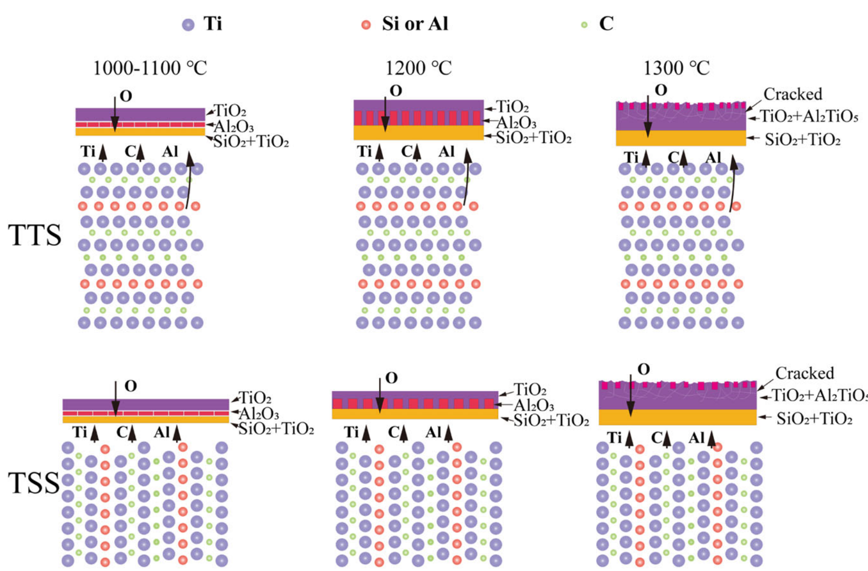

Fig. 13 Schematic illustration of the evolution of the microstructure of oxide scales and an atomistic model describing the formation mechanism of oxide scale on $Ti_3(SiAl)C_2$.

protect the TSS sample from further oxidation. Whereas, the low content of Al in the samples and the retarded diffusion of Al atoms in the TTS sample led to severe oxidation of the TTS sample.

From the above results, we can know that the element Al plays a very important role in the oxidation resistance of textured $Ti_3(SiAl)C_2$. Due to the low content of Al, the ease of its outward diffusion in TTS and TSS determines whether a continuous Al_2O_3 protective layer can be formed. Therefore, the texture affects the oxidation behavior of texture $Ti_3(SiAl)C_2$.

As for Ti_3SiC_2 without Al solid solution, however, its oxidation process was controlled by the inward diffusion of O and the outward diffusion of Ti and C, while Si was kept immobile. This

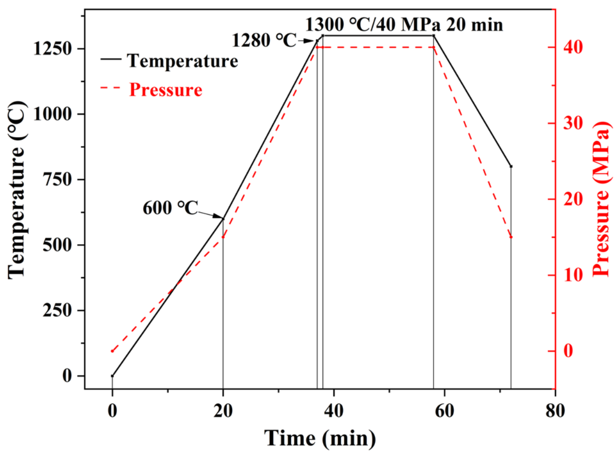

Fig. 14 SPS curves of textured $Ti_3(SiAl)C_2$.

process does not involve the ease of Si external diffusion. Therefore, we can infer that the effect of texture on the oxidation behavior of Ti_3SiC_2 is negligible.

METHODS

Fabrication process

Textured $Ti_3(SiAl)C_2$ ceramic was prepared by a two-step sintering process. Firstly, Ti (~300 mesh, purity: 99.9%), Si (~300 mesh, purity: 99.9%), Al (~300 mesh, purity: 99.9%), and graphite (~300 mesh, purity: 99.99%) powders in a molar ration of 3:1:0.2:2 was used as the raw material for the fabrication of $Ti_3(SiAl)C_2$ powders. In this regard, a small amount of Si was substituted by Al to eliminate TiC impurities and improve its oxidation resistance[6,25,26]. All the elemental powders were placed in an agate ball mill jar and mixed uniformly by planetary ball milling. After ball milling, the mixed powders were placed in a graphite mold and compacted under a pressure of 3 MPa, followed by pressureless sintering at 1450 °C for 1 h in a flowing argon atmosphere. Subsequently, the as-prepared $Ti_3(SiAl)C_2$ was pulverized and ball milled for obtaining fine-grained $Ti_3(SiAl)C_2$ powders. The milling speed and time were 300 rpm and 24 h, respectively. Finally, the fine-grained $Ti_3(SiAl)C_2$ powders were sintered at 1300 °C for 20 min in a vacuum under 40 MPa using an SPS furnace. The SPS curves for $Ti_3(SiAl)C_2$ are shown Fig. 14.

Characterization

The phase compositions of the textured top surface (TTS), textured side surface (TSS), and oxide scales were characterized by XRD (Bruker D8, Germany). Cu-Kα radiation (k = 0.1542 nm) was adopted with a voltage of 40 kV, a current of 40 mA, and a scanning speed of 4o/min. The degree of texture was evaluated by the Lotgering orientation factor, f_L, which can be expressed as:[27]

$$f_L = \frac{P - P_0}{1 - P_0} \tag{5}$$

For a- and b-axes orientations, the values of P and P_0 correspond to the ratio $\sum^{I}_{(hk0)} / \sum^{I}_{(hkl)}$, and for c-axis orientation, the values of P and P_0 correspond to the ratio $\sum^{I}_{(00l)} / \sum^{I}_{(hkl)}$, where $\sum^{I}_{(hko)}$, $\sum^{I}_{(hkl)}$, and $\sum^{I}_{(00l)}$ were the sums of peak intensities of (hko), (hkl), and $(00l)$ planes, respectively. P is from the texture sample and P_0 is from the standard PDF card (74-0310) of $Ti_3(SiAl)C_2$.

The microstructure of the oxidized surfaces, cross-sections, and elemental distributions of textured $Ti_3(SiAl)C_2$ was observed using SEM (Supra 55, Zeiss, Oberkochen, Germany) equipped with EDS (Oxford Instruments, UK). The samples used for SEM analysis and EBSD (Supra 55, Zeiss, Oberkochen, Germany) observation were subjected to standard metallographic procedures, including cutting, grinding and polishing. In addition, the grain structure and the orientation map of the crystal texture were determined by EBSD. The scanning was performed in a hexagonal grid with a step size of 0.2 μm using an accelerating voltage of 20 kV. The sample was tilted by 70° during the EBSD acquisition. The grain boundaries are defined for misorientation angles greater than 5°. The data acquisition and processing were performed using Channel 5 software.

Oxidation tests

Before the oxidation test, the samples with dimensions of $8 \times 8 \times 2\ mm^3$ were cut from the top and side of the textured $Ti_3(SiAl)C_2$ sample, respectively, and then sanded and polished. For the convenience of description, the top surface perpendicular to the compression direction is named TTS and the side surface parallel to the compression direction is named TSS. Regarding the oxidation test of the TTS sample, a pair of faces (8×8), perpendicular to the c-axis, accounted for 66.67% of the total area tested. While for the TSS sample, two pair faces (8×8, and 8×2), parallel to the c-axis, accounted for 83.3% of the total area tested.

The oxidation behavior of textured $Ti_3(SiAl)C_2$ was evaluated using vertical Setsys evolution microbalance (SETARAM, France) in flowing air at 1000–1300 °C for 10 h with a heating rate of 40 °C min^{-1}. The mass change versus oxidation time was recorded continuously with software.

DATA AVAILABILITY

The datasets generated and/or analyzed during the current study are available from the corresponding author on reasonable request.

Received: 24 October 2022; Accepted: 6 March 2023;
Published online: 20 March 2023

REFERENCES

1. Barsoum, M. W. The MN+1AXN phases: a new class of solids: thermodynamically stable nanolaminates. *Prog. Solid State Chem.* **28**, 201–281 (2000).
2. Sokol, M., Natu, V., Kota, S. & Barsoum, M. W. On the chemical diversity of the MAX phases. *Trends Chem.* **1**, 210–223 (2019).
3. Ramachandran, K., Carmine, Z., Yoshida, K., Tsunoura, T. & Jayaseelan, D. D. Experimental investigation and mathematical modelling of water vapour corrosion of Ti_3SiC_2 and Ti_2AlC ceramics and their mechanical behaviour. *J. Eur. Ceram. Soc.* **41**, 4761–4773 (2021).
4. Sun, Z., Zhou, Y. & Li, M. Oxidation behaviour of Ti_3SiC_2-based ceramic at 900-1300 °C in air. *Corros. Sci.* **43**, 1095–1109 (2001).
5. Ji, Y. et al. High temperature oxidation resistance of Ti_3SiC_2 in air and low oxygen atmosphere. *Int. J. Appl. Ceram. Tec.* **14**, 851–859 (2017).
6. Zhang, H. B., Zhou, Y. C., Bao, Y. W. & Li, M. S. Improving the oxidation resistance of Ti_3SiC_2 by forming a $Ti_3Si_{0.9}Al_{0.1}C_2$ solid solution. *Acta Mater.* **52**, 3631–3637 (2004).
7. Zhang, Z. et al. Preparation and anisotropic properties of textured structural ceramics: A review. *J. Adv. Ceram.* **8**, 289–332 (2019).
8. Hu, C. et al. Shell-like nanolayered Nb_4AlC_3 ceramic with high strength and toughness. *Scr. Mater.* **64**, 765–768 (2011).
9. Li, X. et al. Oxidation and creep behavior of textured Ti_2AlC and Ti_3AlC_2. *J. Eur. Ceram. Soc.* **42**, 364–375 (2022).
10. Xu, L. et al. Effect of texture on oxidation resistance of Ti3AlC2. *J. Eur. Ceram. Soc.* **38**, 3417–3423 (2018).
11. Xie, X., Yang, R., Cui, Y. Y., Jia, Q. & Bai, C. G. Fabrication of textured Ti_2AlC lamellar composites with improved mechanical properties. *J. Mater. Sci. Tech.* **38**, 86–92 (2020).
12. Li, X., Xie, X., Gonzalez-Julian, J., Malzbender, J. & Yang, R. Mechanical and oxidation behavior of textured Ti_2AlC and Ti_3AlC_2 MAX phase materials. *J. Eur. Ceram. Soc.* **40**, 5258–5271 (2020).
13. Lapauw, T., Vanmeensel, K., Lambrinou, K. & Vleugels, J. A new method to texture dense $M_{n+1}AX$ ceramics by spark plasma deformation. *Scr. Mater.* **111**, 98–101 (2016).

14. Duan, X. et al. Synthesis of high-purity, isotropic or textured Cr_2AlC bulk ceramics by spark plasma sintering of pressure-less sintered powders. *J. Eur. Ceram. Soc.* **35**, 1393–1400 (2015).
15. Hu, C., Sakka, Y., Grasso, S., Suzuki, T. & Tanaka, H. Tailoring Ti_3SiC_2 ceramic via a strong magnetic field alignment method followed by spark plasma sintering. *J. Am. Ceram. Soc.* **94**, 742–748 (2011).
16. Wang, Q., Li, M.-H., Chen, G.-Q., Fu, X.-S. & Zhou, W.-L. Effects of texture orientation in Ti_3SiC_2 on growth kinetics of interfacial compound layers in diffusion bonded TiAl/Ti_3SiC_2 joints. *J. Eur. Ceram. Soc.* **41**, 244–251 (2021).
17. Li, S., Song, G.-M. & Zhou, Y. A dense and fine-grained SiC/$Ti_3Si(Al)C_2$ composite and its high-temperature oxidation behavior. *J. Eur. Ceram. Soc.* **32**, 3435–3444 (2012).
18. Smialek, J. L. Oxygen diffusivity in alumina scales grown on Al-MAX phases. *Corros. Sci.* **91**, 281–286 (2015).
19. Zuber, A. et al. Towards a better understanding of the high-temperature oxidation of MAX phase Cr_2AlC. *J. Eur. Ceram. Soc.* **42**, 2089–2096 (2022).
20. Smialek, J. L. Kinetic aspects of Ti_2AlC MAX phase oxidation. *Oxid. Met.* **83**, 351–366 (2015).
21. Gao, N. F., Miyamoto, Y. & Zhang, D. On physical and thermochemical properties of high-purity Ti_3SiC_2. *Mater. Lett.* **55**, 61–66 (2002).
22. Chen, J. X. & Zhou, Y. C. Effect of Si content on the oxidation resistance of $Ti_3Al_{1-x}Si_xC_2$ ($x \leqslant 0.25$) solid solutions at 1000–1400 °C in air. *Oxid. Met.* **65**, 123–135 (2006).
23. Zhou, Y. C., Wan, D. T., Bao, Y. W. & Wang, J. Y. In situ processing and high-temperature properties of $Ti_3Si(Al)C_2$/SiC composites. *Int. J. Appl. Ceram. Tec.* **3**, 47–54 (2006).
24. Wang, X. H. & Zhou, Y. C. Stability and selective oxidation of aluminum in nano-laminate Ti_3AlC_2 upon heating in argon. *Chem. Mater.* **15**, 3716–3720 (2003).
25. Zheng, L.-L., Sun, L.-C., Li, M.-S. & Zhou, Y.-C. Improving the high-temperature oxidation resistance of $Ti_3(SiAl)C_2$ by Nb-doping. *J. Am. Ceram. Soc.* **94**, 3579–3586 (2011).
26. Guedouar, B. et al. Oxidation behavior of Al-doped Ti_3SiC_2-20 wt.%Ti_5Si_3 composite. *Ceram. Int.* **47**, 33622–33631 (2021).
27. Zhu, X. & Sakka, Y. Textured silicon nitride: processing and anisotropic properties. *Sci. Technol. Adv. Mater.* **9**, 033001 (2008).

ACKNOWLEDGEMENTS

This work was supported by the National Natural Science Foundation of China (Grant No. 52071318) and the Fund of Science and Technology on Advanced Functional Composites Laboratory (Grant No. 6142906210305).

AUTHOR CONTRIBUTIONS

G.Q.H. designed the experiments, analyzed the results, and wrote the paper. X.T.Z., W.T.W., K.M., and J.Z. contributed to the experiments of the TG, XRD, SEM, EBSD, and its data processing. M.S.L., C.S.L., and J.J.X. revised the paper. All the authors contributed to the interpretation of the experimental data.

COMPETING INTERESTS

The authors declare no competing interests.

ADDITIONAL INFORMATION

Correspondence and requests for materials should be addressed to Jingjun Xu.

Reprints and permission information is available at http://www.nature.com/reprints

Publisher's note Springer Nature remains neutral with regard to jurisdictional claims in published maps and institutional affiliations.